ACKNOWLEDGMENT

The authors are grateful to K. B. Niclas of Watkins-Johnson Company for making available the device data for the results reported in Fig. 4.

REFERENCES

[1] K. W. Kobayashi, R. Esfandiari, W. L. Jones, K. Minot, B. R. Allen, A. Freudenthal, and D. C. Streit, "A 6–21-GHz monolithic HEMT 2×3 matrix distributed amplifier," *IEEE Microwave Guided Wave Lett.*, vol. 3, pp. 11–13, Jan. 1993.

[2] R. Heilig, D. Hollman, and G. Baumann, "A monolithic 2–52 GHz HEMT matrix distributed amplifier in coplanar waveguide technology," in *IEEE MTT-S Int. Microwave Symp.*, San Diego, CA, 1994, pp. 459–462.

[3] S. D'Agostino, G. D'Inzeo, G. Gatti, and P. Marietti, "A low-DC power 2–18 GHz monolithic matrix amplifier," in *IEE Proc. Microwave Antennas and Propagation*, Dec. 1994, pp. 440–444.

[4] K. B. Niclas and R. R. Pereira, "The matrix amplifier: A high-gain module for multioctave frequency bands," *IEEE Trans. Microwave Theory Tech.*, vol. MTT-35, pp. 296–306, Mar. 1987.

[5] C. Paoloni and S. D'Agostino, "An approach to distributed amplifier based on a design-oriented FET model," *IEEE Trans. Microwave Theory Tech.*, pp. 272–277, Feb. 1995.

[6] S. D'Agostino, G. D'Inzeo, G. Grifoni, P. Marietti, and G. Panariello, "A 0.5–12 GHz hybrid matrix distributed amplifier using commercially available HEMT's," in *IEEE MTT-S Int. Microwave Symp.*, Boston, MA, 1991, pp. 289–292.

[7] S. L. G. Chu, Y. Tajima, J. B. Cole, A. Platzker, and M. J. Schindler, "A novel 4–18 GHz monolithic matrix distributed amplifier," in *1989 IEEE MTT-S Int. Microwave Symp. Dig.*, June 1989, pp. 291–295.

[8] A. P. Chang, K. B. Niclas, B. D. Cantos, and W. A. Strifler, "Monolithic 2–18 GHz matrix amplifiers," *IEEE Trans. Microwave Theory Tech.*, vol. 37, pp. 2159–2162, Dec. 1989.

[9] J. B. Beyer, S. N. Prasad, R. C. Becker, J. E. Nordman, and G. K. Hohenwarter, "MESFET distributed amplifier guidelines," *IEEE Trans. Microwave Theory Tech.*, vol. MTT-32, pp. 268–275, Mar. 1984.

[10] R. Dixit, B. Nelson, W. Jones, and J. Carillo, "A family of 2–20 GHz broadband low noise AlGaAs HEMT MMIC amplifiers," in *1989 IEEE Microwave and Millimiter-Wave Monolithic Circuits Symp. Dig.*, June 1989, pp. 15–19.

Calculation of Distributed Capacitances of Spiral Resonators

Zunfu Jiang, P. S. Excell, and Z. M. Hejazi

***Abstract*— A method for calculating the distributed capacitances and resonant frequencies of spiral resonators is described. First, the charge distribution on a spiral is found by a simplified model and the moment method, then the distributed capacitance is calculated. The equivalent inductance of the spiral resonator is then evaluated according to a standard formula, and the resonant frequencies are finally computed. The calculated results are compared with experimental data, and a good agreement between them is shown.**

I. INTRODUCTION

Planar spirals have certain advantages as electrically small resonators, but their characteristics are not well understood and empirical design methods tend to be used. Experimental results for some characteristics of planar spiral resonators are described in [1]. The equivalent circuit of a planar spiral resonator can be made up of an inductance, a capacitance, and a resistance. The inductances of thin-film planar spirals are considered in [2]–[4]. An empirical formula, with limited accuracy, for calculating the distributed capacitance of planar spirals is given in [5] as

$$C = 0.035 D_o + 0.06 \quad [\text{pF}] \tag{1}$$

where D_o is the outer diameter of the spiral in millimeters. This formula is only approximate as it clearly neglects several relevant parameters.

The inductance and resistance of a planar spiral resonator can be computed with sufficient accuracy from the available literature. While the resonant frequencies of spiral inductors can also be predicted using standard software packages, there is a high cost in computational time and it is useful to have analytical expressions if they can be found. For this, a simple effective method for the capacitance is the main need.

In this paper, a method for calculating distributed capacitances and resonant frequencies of spiral resonators is described. First, the charge distributions on the spirals are found by a simplified model and the moment method. Then, the distributed capacitances of the spiral resonators are calculated. The equivalent inductances of the spiral resonators are then evaluated according to a standard formula and the resonant frequencies are finally computed and compared with experimental data from Nishi *et al*. [1].

II. CALCULATION OF THE DISTRIBUTED CAPACITANCE

A planar spiral resonator system includes a spiral on a substrate, coupling circuits, and a shield box. For simplicity, a spiral in a uniform dielectric medium with permittivity ε is considered and is illustrated, with an equivalent circuit, in Fig. 1.

It is assumed that the capacitance C_o per unit length of the spiral resonator is given (see Section III). Following the method described in [8], the total distributed capacitance C of the spiral resonator can be

Manuscript received October 17, 1995; revised September 23, 1996.

Z. Jiang is with the Institute of Electronics, Academia Sinica, Beijing 100080, China.

P. S. Excell and Z. M. Hezaji are with the Department of Electronic and Electrical Engineering, University of Bradford, Bradford BD7 1DP, U.K.

Publisher Item Identifier S 0018-9480(97)00278-0.

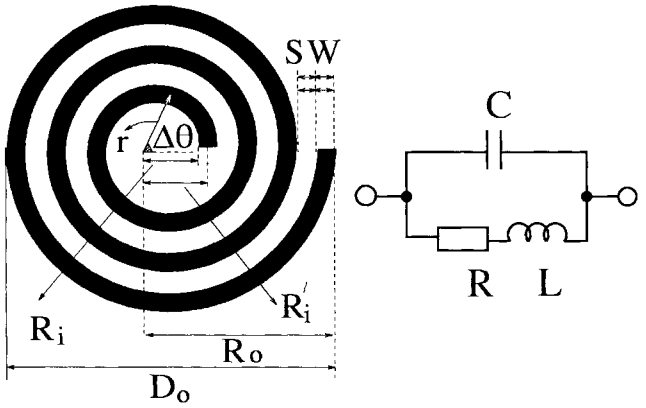

(a) (b)

Fig. 1. Layout of a spiral resonator and its equivalent circuit. (a) The physical layout. (b) Equivalent circuit.

found. If the width W of the spiral conductors is equal to the spacing S between the turns, the equation of the spiral is $r = R_i' + W\theta/\pi$. R_i' is the initial mean radius, which is equal to $R_i + W/2$, R_i is the inner initial radius, r is the mean radius, and θ is the rotational angle in radians (see Fig. 1).

The voltage between the ends of the spiral with N turns is denoted by U. Then, the voltage per turn is U/N, and the distributed capacitance of the spiral is

$$C = \frac{q}{U} = \frac{1}{U}\int_0^{2\pi N} \frac{U}{N} C_o\left(R_i' + W\frac{\theta}{\pi}\right)d\theta \tag{2}$$

hence

$$C = \pi\, C_o(R_i + R_o) \tag{3}$$

where R_o is the outer final radius of the spiral. This formula is obtained under the assumption that C_o is independent of r.

III. Calculation of the Capacitance C_o

A. Green's Function

The geometric formation of a spiral is approximately axisymmetric [3]. The potential function in the space occupied by it is also symmetric in a cylindrical coordinate system. Therefore, each turn of the spiral can be substituted by a circular loop with an appropriate radius. The capacitance C_o can be computed from two circular loops with the same width W and spacing S. The Green's function of a circular wire loop with radius r_o and a line charge density ρ in a homogeneous dielectric with permittivity ε can be given by [7]

$$G(r,z;r_o,z_o) = \begin{cases} \frac{1}{2\pi\varepsilon}\sqrt{\frac{r_o}{r}}kF(k), & r \neq 0 \\ \frac{r_o}{2\varepsilon\sqrt{r_o^2+(z-z_o)^2}}, & r = 0 \end{cases} \tag{4}$$

where

$$k^2 = 4r_o r/(r_o + r)^2 + (z - z_o)^2. \tag{5}$$

$F(k)$ is the complete elliptic integral of the first kind with modulus k, and (r,z) is the coordinate of any point P.

For two thin annular rings [see Fig. 2(b)], the total potential at an arbitrary point $P(r,z)$ is

$$V_t = \int_{r_1}^{r_2} G_1(r,z;r_o,z_o)\rho_1(r_o,z_o)dr_o + \int_{r_3}^{r_4} G_2(r,z;r_o',z_o')\rho_2(r_o',z_o')dr_o' \tag{6}$$

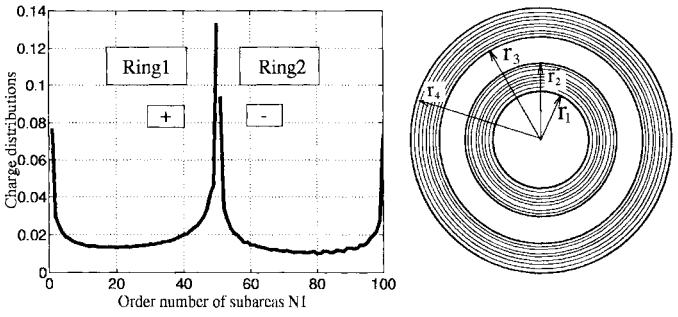

(a) (b)

Fig. 2. (a) Charge distributions on two rings. (b) The geometry of two annular rings.

where G_1, G_2, and ρ_1, ρ_2 are the Green's functions and charge distribution functions, respectively. The inner and outer rings have similar mathematical formulations.

B. Charge Distribution

When the point $P(r,z)$ is taken on the surface of the inner or outer ring, the voltage on the surface of the ring can be obtained from (6). Since the two rings are taken to be perfect conductors, the tangential electric fields on their surfaces must be zero, i.e., the potential of every point on the surface of each ring must be equivalent. This condition can be obtained by adjusting the charge distribution on each ring. If the voltages on the surfaces of both rings are given as $+V$ and $-V$, respectively, then the charge distributions on both ring surfaces can be solved from (6).

The integrals can easily be solved by a straightforward numerical technique or the moment method. First, each conductor ring surface is subdivided into N_1 sub-annuli of finite width H_i, and every sub-annulus of ring 1 and ring 2 is denoted as $1, 2, \cdots, N_1$ and $N_1 + 1, N_1 + 2, \cdots, 2N_1$, respectively. The charge distribution on each sub-annulus surface is assumed to be constant. Secondly, suppose the voltage on one sub-annulus H_j equals V_j, which should be a result of the charge distribution on this sub-annulus as well as on all the other sub-annuli. The voltage V_j for $j = 1, 2, \cdots, 2N$ can be written in matrix form as

$$[A][\rho] = [V] \tag{7}$$

where $[V]$ and $[\rho]$ are column matrices and $[A]$ is a matrix $2N_1 \times 2N_1$ with matrix elements A_{ji}. From (6), A_{ji} can be represented as

$$A_{ji} = \frac{Hr_i}{\pi\varepsilon(r_i + r_j)}F[k(j,i)] \quad k_{ji} = \frac{2\sqrt{r_i r_j}}{r_i + r_j}. \tag{8}$$

When i equals j, the function $F[k(j,i)]$ will have singular points and must be treated separately. This case finds the voltage of a sub-annulus loop of radius r_i at its own position.

Assume that a sub-annulus loop with inner radius r and outer radius $r + \Delta r$ has a surface charge distribution ρ and is itself divided into M subareas. The area of each subarea is $r\Delta\theta\Delta r$, so that the charge quantity on the surface of each subarea is $\alpha_o = \rho\, r\Delta\theta\, \Delta r$. The potential produced by the ith subarea charge element at the position of the jth subarea element can be given as [9]

$$V_{ji} = \frac{1}{4\pi\varepsilon}\frac{\alpha_o}{\sqrt{2}r\sqrt{1 - \cos[(j-i)\Delta\theta]}}. \tag{9}$$

The total potential at the position is

$$V_j = V_{1j} + V_{2j}$$

where

$$V_{1j} = \sum_{i=1}^{M} \frac{1}{4\pi\varepsilon} \frac{\rho r \Delta\theta \Delta r}{\sqrt{2} r \sqrt{1-\cos[(j-i)\Delta\theta]}}, \quad i \neq j \tag{10}$$

and V_{2j} is the potential for $i = j$. When $r\Delta\theta$ is taken to be equal to Δr, for $i = j$, V_{2j} can be given as [9]

$$V_{2j} = \rho \frac{\Delta r}{\pi\varepsilon} \ln(1+\sqrt{2}). \tag{11}$$

From (10), the matrix elements A_{jj} in (7) can then be written as

$$A_{jj} = \frac{H}{\pi\varepsilon} \ln(1+\sqrt{2}) + \frac{H^2}{4\pi\varepsilon\sqrt{2}r} \sum_{i=1}^{M} \frac{1}{\sqrt{1-\cos[(j-i)\Delta\theta]}} \tag{12}$$

where $i \neq j$. Let V in (7) be equal to one, it can now be solved for the charge densities $[\rho]$ by inversion of the matrix $[A]$ or by using numerical techniques to solve the simultaneous equations. From the solved charge densities $[\rho]$ and the charge quantity q on the ring 1 is

$$q = \sum_{i=1}^{N_1} \rho_i 2\pi r_i H. \tag{13}$$

The distributed capacitance between both rings is

$$C_1 = \frac{1}{2} q = \pi H \sum_{i=1}^{N_1} r_i \rho_i \tag{14}$$

and the capacitance C_o per unit length is

$$C_o = C_1 / 2\pi r. \tag{15}$$

IV. Numerical Computation and Results

The spiral resonator structure measured in [1] is used in our calculations where shield diameter $D_s = 30$ mm with removed top cover. The dimensions of the spiral resonators were as follows: Outer diameters of the spirals are $D_o = 20$ and 10 mm, respectively; the ratio between inner and outer diameters was $D_i/D_o = 0.2$; the ratio between the width W and spacing S of the spirals was $W/S = 1$; the number of turns was $N = 3, 4, 5, 7, 10$; the thickness of the substrate $t_s = 0.62$ mm and the dielectric constant of the substrate was $\varepsilon_r = 9.5$. The width W of the spirals' conductors was found from $W = (D_o - D_i)/(4N+2)$. The coupling to the spirals was via grounded semi-loop strips connected with coaxial lines from both sides. Substituting (15) in (3), the distributed capacitance of the spiral resonators can be found from

$$C = C_1 (R_i + R_o)/2r \tag{16}$$

where r is the mean radius of the rings. If r is selected to be equal to $(R_i + R_o)/2$, then we have $C = C_1$ and the dimensions of two rings having an equivalent capacitance of a desired spiral can be found as

$$r_1 = [(D_o + D_i) - 6W]/4. \tag{17}$$

$C = C_1$ is an interesting result showing that the distributed capacitance of a spiral with N turns is equal to the capacitance between two annular rings (with radii found as shown below) and independent of its turns' number N. Therefore, in our computation, the radii of two annular loops were $r_i = r_1 + (i-1)W$, where $i = 1, 2, 3, 4$.

To achieve good accuracy, each annular loop is divided into $N_1 = 50$ sub-annular loops. According to the condition $r\Delta\theta = \Delta r$, M in (10) should be taken as the integer part of $M_1 = 2\pi N_1 r_i / W$. The effective Dielectric Constant ε_{eff} for suspended strip lines with $W/h < 1$ can be calculated from [10]. Fig. 2 shows the calculated charge distribution for two annular loops. The abscissa values are n, which represent the radii of the loops that can be expressed for ring 1 as $r = r_i + nH$ $(n = 1, 2, \cdots, 50)$ and for ring 2 as $r = r_i + 2W + nH$ $(n = 51, 52, \cdots, 100)$, respectively. Fig. 3 shows the calculated and experimental resonant frequencies for five different spiral resonators. It is seen that the agreement between both is good. Fig. 4 shows the calculated distributed capacitances. It is seen that the distributed capacitance under this condition $(D_o/D_i = \text{const.})$ is very weakly dependent on the number of turns N of the spiral. This was corroborated by the experimental results. This may be due to the nonuniformity of the current distribution along the spiral. The greatest density thus tends to be in the central part where the inter-turn capacitances can be treated as parallel while the outer turns' capacitances are effectively in series: a certain compensation possibly occurs.

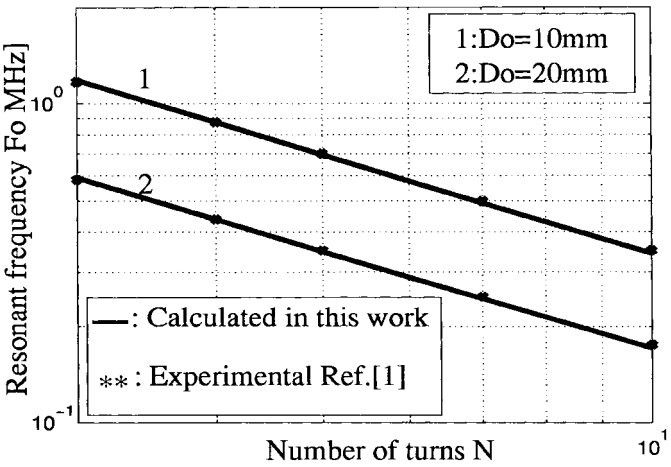

Fig. 3. Resonant frequency versus number of turns with two different outer diameters.

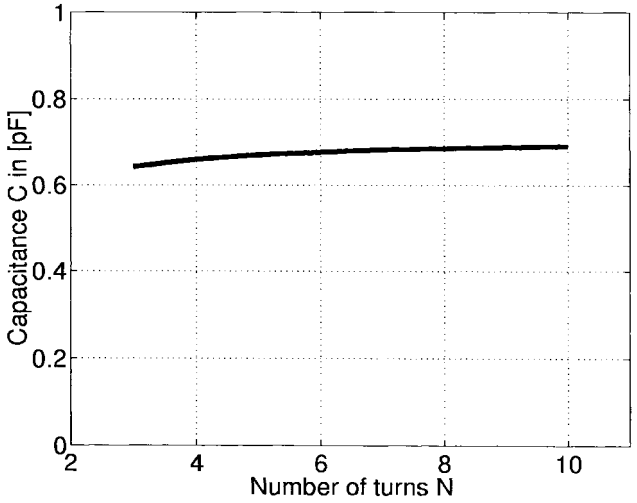

Fig. 4. Distributed capacitances versus number of turns in the spiral.

V. Conclusion

A method for calculating the distributed capacitances and resonant frequencies of spiral resonators has been presented and indicated to be effective from the good agreement between computed and experimental results. Though the method is approximate and simple, good accuracy of calculation can be achieved with a modest computational task. However, it should be noted that the calculated distributed capacitance does not include the fringing end-effect capacitance and the shield case. The end capacitance is negligibly small in the case of suspended striplines. Our current experiments show that the shield case influences F_o by $\approx$1.5%. More accurate evaluation of these effects and others will be published in due course.

REFERENCES

[1] I. Nishi, K. Yanagisawa, and T. Toshima, "Spiral resonator for PCM-400 M system," *Rev. Elect. Comm. Lab.*, vol. 24, nos. 9–10, pp. 776–786, 1976.

[2] A. Olivei, "Optimized miniature thin-film planar inductors compatible with integrated circuits," *IEEE Trans. Parts, Hybrids, Packag.*, vol. PHP-5, pp. 71–88, June 1969.

[3] Y. Midorikawa, I. Marinova, S. Hayano, and N. Yaito, "Electromagnetic field analysis of film transformer," *IEEE Trans. Magn.*, vol. 31, pp. 1456–1459, May 1995.

[4] M. Caulton, S. P. Knight, and D. A. Daly, "Hybrid integrated lumped-element microwave amplifiers," *IEEE Trans. Electron Devices*, vol. ED-15, pp. 459–466, July 1968.

[5] R. S. Pengelly and D. C. Richard, "Design, measurement and application of lumped elements up to J-band," in *Proc. 7th Europ. Microwave Conf.*, Copenhagen, Denmark, 1977, pp. 460–464.

[6] K. C. Gupta, R. Garg, and R. Chadha, *Computer-Aided Design of Microwave Circuits*. Norwood, MA: Artech House, 1981, pp. 211–212.

[7] R. Chadha and K. C. Gupta, "Green's functions for circular sectors, annular rings and annular sectors in planar microwave circuits," *IEEE Trans. Microwave Theory Tech.*, vol. 29, pp. 68–71, Jan. 1981.

[8] A. J. Palermo, "Distributed capacity of single layer coils," *Proc. IRE*, vol. 22, pp. 897–909, 1934.

[9] R. E. Harrington, *Field Computation by Moment Methods*. Malabar, FL: Krieger, 1985, p. 27.

[10] J. M. Schallenberg, "CAD models for suspended and inverted microstrip," *IEEE Trans. Microwave Theory Tech.*, vol. 43, pp. 1247–1254, June 1995.

Design of Modified Phase Reversal Electrode in Broad-Band Electrooptic Modulators at 100 GHz

Kwok-Wah Hui, B. Y. Wu, Y. M. Choi, J. H. Peng, and K. S. Chiang

***Abstract*—An analysis is given on the modified phase reversal structure of electro-optic modulators. It is shown that the bandwidth to half-wave voltage ratio (BVR) increases with the number of phase reversal sections. Under the assumption that the number of electrode sections is M, a set of M-elements second-order nonlinear equations has been derived and solved by Newton's iteration method. The calculated results provide the optimum overlap integral for each section of a phase reversal modulator in order to "flatten" the frequency response of the device.**

***Index Terms*—Integrated optics, optical modulators, optimization.**

I. INTRODUCTION

The bandwidth of integrated electrooptic modulators is limited mainly by the transmission attenuation and the mismatch between the optical and microwave velocities [1]–[3]. To increase the bandwidth, the length of the electrode needs to be reduced. This will, however, in turn increase the half-wave voltage, V_π [4]. In the past few years, a number of modulators have been built using techniques such as "thick electrode" and "ridge structure" to eliminate the velocity mismatch between optical and microwave signals [5], [6]. Although in these modulators the length of the electrode can be increased to maximize the response of the device, their electrode structures are rather complicated and would be more difficult to fabricate. An alternative to increase the BVR is the use of the phase reversal electrodes [7]. There are different types of phase reversal electrodes [8], [9]. These include the periodic and nonperiodic types, the continuous function, and the simple step function electrodes. Each of them provides a certain degree of improvement on the flatness of the frequency response with significant increase in bandwidth to half-wave voltage ratio (BVR) [10]. This paper will concentrate on the nonperiodic step function electrode because it has a flat frequency response and is easier to fabricate when compared with the continuous function electrode, thick electrode, and ridge structure. The electrode is divided into M sections of equal length. Mathematical analysis yields a set of M-elements second-order nonlinear equations that is then solved by Newton's iteration method. The figure of merit, Q, can then be computed. Here, Q is defined as the ratio of the BVR for an electro-optic modulator with M sections of electrodes to that of a conventional electro-optic modulator (with only one section of electrode).

Manuscript received December 4, 1995; revised September 23, 1996.

K.-W. Hui and K. S. Chiang are with the Department of Electronic Engineering, City University of Hong Kong, Hong Kong.

B. Y. Wu and J. H. Peng are with the Department of Electronic Engineering, Tsinghua University, Beijing, China.

Y. M. Choi is with the ISO-Ing Centre, Hong Kong.

Publisher Item Identifier S 0018-9480(97)00279-2.

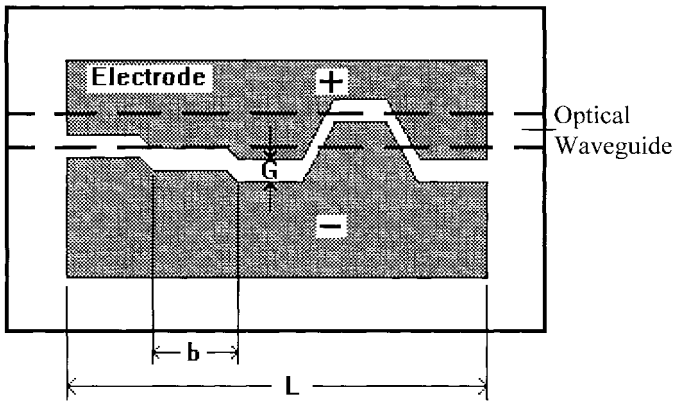

Fig. 1. Schematic diagram of phase modulator with five sections of phase reversal electrode.

II. ELECTRODE STRUCTURE

Fig. 1 shows the schematic diagram of a five-section phase modulator. An electrode of length L is divided into M sections of equal length. The length of each section, b, is, therefore, equal to L/M. This structure employs a simple step function and provides a flat frequency response. The electro-optic overlap integral at the ith section is Γ_i where $i = 1, 2, \cdots, M$. In general, different sections of i have different Γ_i since the relative position between the central line of the electrode gap, G, and that of the optical waveguide varies in different sections. The relative position between the central lines in each section, however, is constant. This type of electrode pattern is called the step electrode structure.

III. MATHEMATICAL ANALYSIS

For a phase reversal structure in which the microwave phase is reversed at the end of each section, the total induced optical phase shift ϕ is given by [8]

$$\frac{\phi(f)}{FL} = \frac{1}{\gamma L}\sum_{i=1}^{M}\Gamma_i\left[e^{-\gamma(i-1)b} - e^{-\gamma ib}\right] \tag{1}$$

where

$\phi(f)$ function of the modulating frequency, f_m;
F $= (-n_o^3 r E_m \pi/\lambda)\exp(j\omega t_0)$;
n_o effective refractive index for the optical wave;